Phys. Status Solidi C **12**, No. 4–5, 469–472 (2015) / **DOI** 10.1002/pssc.201400154

physica status solidi c
www.pss-c.com
current topics in solid state physics

STEM-CL investigations on the influence of stacking faults on the optical emission of cubic GaN epilayers and cubic GaN/AlN multi-quantum wells

R. M. Kemper[1], P. Veit[2], C. Mietze[1], A. Dempewolf[2], T. Wecker[1], F. Bertram[2], J. Christen[2], J. K. N. Lindner[1], and D. J. As[*,1]

[1] Universität Paderborn, Department Physik, Warburger Str. 100, 33098 Paderborn, Germany
[2] Universität Magdeburg, Institut für Festkörperphysik, P.O. Box 4120, 39016 Magdeburg, Germany

Received 27 June 2014, revised 30 January 2015, accepted 15 February 2015
Published online 4 March 2015

Keywords cubic GaN, STEM-CL, molecular beam epitaxy

[*] Corresponding author: e-mail d.as@uni-paderborn.de, Phone: +49 5251 60 5838, Fax: +49 5251 60 5843

We report the influence of {111} stacking faults on the cathodoluminescence (CL) emission characteristics of cubic GaN (c-GaN) films and cubic GaN/AlN multi-quantum wells. Transmission electron microscopy (TEM) measurements indicate that stacking faults (SFs) on the {111} planes are the predominant crystallographic defects in epitaxial films, which were grown on 3C-SiC/Si (001) substrates by plasma-assisted molecular beam epitaxy. The correlation of the SFs and the luminescence output is evidenced with a CL setup integrated in a scanning TEM (STEM). By comparing the STEM images and the simultaneously measured CL signals it is demonstrated that SFs in these films lead to a reduced CL emission intensity. Furthermore, the CL emission intensity is shown to increase with increasing film thickness and decreasing SF density. This correlation can be connected to the reduction of the full width at half maximum of X-ray diffraction rocking curves with increasing film thickness of c-GaN films.

© 2015 WILEY-VCH Verlag GmbH & Co. KGaA, Weinheim

1 Introduction Group III-nitrides, like GaN, AlN and their alloys are qualified for highly efficient optoelectronic and high-power devices operating at high temperatures. Moreover, due to the relatively large difference in the band gap energy between GaN and AlN these semiconductor materials are promising candidates for novel nitride devices like quantum well infrared photodetectors (QWIP) and quantum cascade lasers (QCL).

Commonly, the thermodynamically stable wurtzite (WZ) phase of GaN is used for device fabrication. But the WZ phase has piezoelectric polarization fields along its c-axis, resulting in limited performances of optoelectronic devices. In contrast, the meta-stable zinc blende (ZB) (or cubic) phase is free of such effects because of its more symmetric crystal structure. This is why the non-polar and semi-polar systems have obtained a growing interest in recent years [1]. In the ZB system Tschumak et al. [2] presented the first field effect transistor and Mietze et al. [3] and Zainal et al. [4] demonstrated resonant tunnel diodes fabricated from cubic GaN (c-GaN).

One of the key issues in device fabrication is the improvement of the structural quality, which can be enhanced if devices are fabricated on lattice-matched substrates. Due to a lack of c-GaN bulk substrates [5] 3C-SiC (001) with a mismatch of about -3.2% between c-GaN and 3C-SiC is the substrate of choice. Transmission electron microscopy (TEM) images provide the evidence that stacking faults (SFs) on the {111} planes are the predominant crystallographic defects in c-GaN films [6, 7]. These SFs are local deviations from the cubic (111) stacking sequence *ABCABC* resulting in a hexagonal (0001) stacking sequence *ABAB* as in the WZ phase. Therefore, SFs can be considered as hexagonal inclusions in a cubic matrix [8]. In the opposite case, basal-plane SFs in a WZ crystal also produce cubic inclusions in the hexagonal crystal structure. In the WZ phase the role of

© 2015 WILEY-VCH Verlag GmbH & Co. KGaA, Weinheim

extended defects [9] and the emission lines from SFs have already been studied in detail [10-13].

Until now the direct influence of planar defects on the CL emission characteristics of c-GaN films and asymmetric cubic GaN/AlN multi-quantum wells (c-GaN/AlN MQWs) is not reported. Therefore, we investigate the correlation between {111} SFs and the emission intensity of c-GaN and c-MQW films by simultaneously measuring scanning TEM (STEM) images and CL signals [14].

2 Experimental The cubic III-nitrides were grown by plasma-assisted molecular beam epitaxy (MBE) on 12 µm thick 3C-SiC (001) layers which were deposited by low-pressure chemical vapor deposition on a 500 µm Si (001) substrate [15]. The growth of c-GaN and c-AlN was realized under one monolayer of Ga or Al on the surface, respectively. Absorption and desorption of the Ga and the Al layers were monitored by *in-situ* reflection high-energy electron diffraction. Details about the optimized growth conditions can be found in Ref. [16, 17].

Two types of samples were fabricated with structures as displayed in Fig. 1. The growth direction is [001]. Samples of the first type consist of a simple thin film of c-GaN on a 3C-SiC/Si (001) substrate. Sample A is of this type and has a thickness of 450 nm. Sample B is built up of a 50 nm c-GaN buffer layer on the 3C-SiC/Si (001) substrate followed by 40 periods of asymmetric QWs. The active region is embedded in 3 nm c-AlN barriers and formed by a 2.1 nm c-GaN QW coupled by a 0.9 nm c-AlN barrier with a 1.6 nm c-GaN QW. Altogether the c-MQW film on top of the c-GaN buffer has a thickness of around 300 nm.

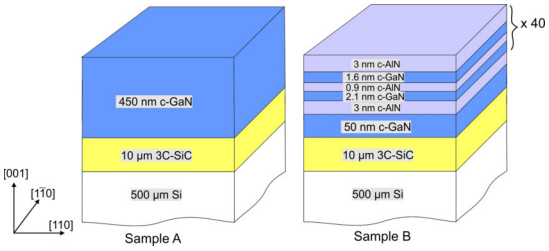

Figure 1 Structure of sample A and B.

The samples were characterized by simultaneously measuring STEM images and CL signals at room temperature and 16 K. The samples were prepared by conventional cross-section preparation with mechanical grinding and polishing followed by an ion beam thinning step. Before STEM analysis the samples were cleaned in an oxygen plasma and then examined in a Tecnai F20 (S) TEM operating at 80 kV with an integrated CL setup [18]. The CL system is equipped with a Mono CL4 mono-chromator from Gatan, a GaAs photomultiplier from Hamamatsu and for parallel detection a SPEX 10-100B CCD from Princton Instruments and has an excitation resolution of about 1 nm at room temperature and < 5 nm at 12 K. The lateral resolution of the CL signal with an estimated specimen thickness of 150-200 nm of the cross-section TEM specimens is determined to about < 20 nm. The effect of charge carrier diffusion is not quantified here.

3 Results and discussion

3.1 GaN samples Figure 2 shows a cross-section STEM annular dark field (ADF) image along the [110] zone axis of sample A. The 450 nm thin c-GaN epilayer on top of the 3C-SiC substrate is shown. Planar defects, identified as SFs on the {111} planes, extend from the c-GaN/SiC interface with an inclination of 57.4° towards

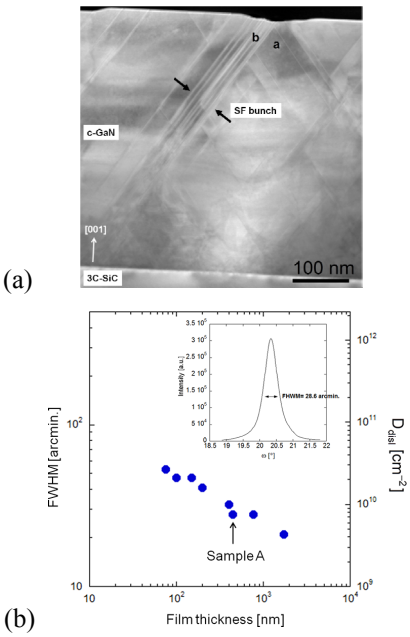

Figure 2 (a) Cross-sectional STEM image along the [110] zone axis of sample A. Individual and also bunches of SFs run from the c-GaN/3C-SiC (001) interface to the c-GaN surface. (b) Rocking curve line width of c-GaN epilayers grown on 3C-SiC/Si (001) substrates plotted *versus* the film thickness of c-GaN epilayers and the associated dislocation density N_{disl} determined by the method of Gay et al. [21]. The inset shows the X-ray rocking curve of sample A.

the sample surface. Individual and also bunches of SFs can be observed. A general tendency that the SF density is reduced with increasing film thickness is clearly observable. This trend is caused by annihilation mechanisms where two SFs, lying on different {111} lattice planes inclined to each other, intersect and annihilate simultaneously, resulting in improved crystalline quality towards the sample surface. A systematic decrease of the SF density as a function of layer thickness has been verified by Martinez-Guerrero et al. [19].

Moreover, the glide model by Ayers [20] implies that the dislocation density N_{disl} is inversely proportional to the layer thickness *d*. This can be proved performing high-resolution X-ray diffraction (HRXRD) rocking curves and

© 2015 WILEY-VCH Verlag GmbH & Co. KGaA, Weinheim

using the model of Gay et al. [21] which connects the rocking curve (ω-scan) line width with the dislocation density N_{disl}. In Fig. 2(b) the full width at half maximum (FWHM) of the (002) rocking curves of c-GaN epilayers grown on 3C-SiC/Si (001) substrates is plotted versus the layer thickness and the associated dislocation density N_{disl}. The plot unambiguously shows that the FWHM decreases with increasing epilayer thickness, indicating a correlation between the FWHM, respectively the dislocation density N_{disl}, and the film thickness. Similar results for c-GaN layers on 3C-SiC (001) substrates are reported in [22]. The inset exemplarily reveals the rocking curve of sample A with a FWHM of ~29 arcmin corresponding to a dislocation density N_{disl} in the order of 10^{10} cm^{-2}.

3.2 Cubic GaN/AlN MQWs Since MQW samples exhibit particulary strong luminescence, a c-GaN/AlN MQW film (sample B) is used for STEM/CL measurements. Figure 3a shows a cross-sectional high-angle annular dark field (HAADF) STEM image taken along the [110] zone axis of sample B. On top of the 50 nm c-GaN buffer the MQW layer stack can be seen. In the HAADF-STEM mode the c-GaN layers can clearly be distinguished from c-AlN by their higher intensity. The STEM image shows slight image distortions in the vertical scanning direction, visible by the rough appearance of the atomically sharp GaN/SiC interface. Besides the image distortions the entire MQW film exhibits undulations of the individual MQW layers. These undulations are caused by the surface morphology of the c-GaN buffer and by bunches of SFs extending from the c-GaN/SiC interface up to the surface, as previous TEM studies [23] have shown.

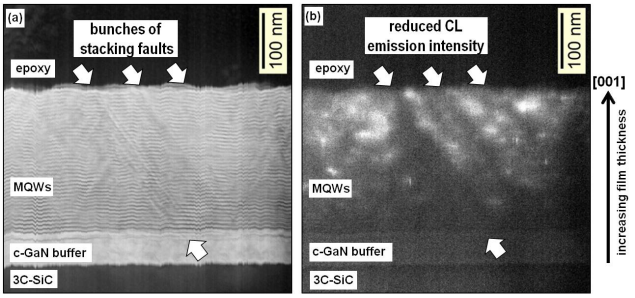

Figure 3 (a) Cross-sectional STEM image in HAADF contrast along the [110] zone axis of sample B. (b) Corresponding panchromatic image of the CL signal at room temperature.

These TEM studies also revealed that SFs emerging from the substrate interface are not stopped at the c-AlN/GaN interfaces of the different layers and lead to the undulation of MQWs. In regions without planar defects a straight sequential arrangement of c-GaN and c-AlN layers can be noticed with equal growth rate [23]. Again, a decreasing SF density with increasing film thickness due to annihilation processes can be noticed. To analyze the influence of SFs on the luminescence output of the MQW film a panchromatic image within a wavelength range of 160-930 nm of the CL emission intensity is displayed in Fig. 3b. This image is spatially correlated to the STEM image in Fig. 3a and both images were collected simultaneously at room temperature.

Figure 3b reveals an inhomogeneous distribution of the CL emission intensity. The spatial correlation of Fig. 3a and b shows that the emission intensity increases with increasing MQW film thickness, i.e. towards the sample surface. High emission intensities (hot spots) appear in regions with a lower defect density, which are mostly located near the sample surface. In regions with bunches of SFs (marked by white arrows in Fig. 3a and b, the intensity of the CL signal is much lower and no hot spots can be detected. In these regions, non-radiative recombination seems to be the predominant exciton annihilation process. One reason for this could be non-radiative recombination centers induced by SFs. These measurements directly demonstrate a correlation between the CL emission intensity and the film thickness dependent crystal quality.

Another reason for the reduced CL intensity may be the type I band alignment of the wider band gap of the WZ GaN phase ($E_g = 3.4$ eV) compared to the cubic phase ($E_g = 3.2$ eV) [24]. Carriers induced in the WZ phase will diffuse into the surrounding cubic matrix with the smaller band gap which lowers the emission from the hexagonal inclusions.

Room temperature CL spectra obtained by exciting different regions (marked by 1-4 in the STEM image (Fig. 4b)) are displayed in Fig. 4a. The CL emission spectrum at position 1 belongs to the 3C-SiC substrate, at position 2 to the c-GaN buffer layer, position 3 to the area of the first c-AlN layer embedded in c-GaN and position 4 was taken from the MQW layer near the surface of the sample, respectively. All emission spectra contain two dominant peaks at 3.26 eV and 3.64 eV plus the emission from the deep compensating complex in the range from 2.3-2.9 eV. The peak at 3.26 eV is due to the radiative recombination of the free exciton (FX) transition in c-GaN [23], and the emission peak at 3.64 eV can be related to the asymmetric coupled c-MQWs [25]. The transition energies of the QWs have been simulated by the *nextnano*[3] software [26] and the calculations (not shown here) agree very well with the observed transitions. The emission is assigned to the wider 2.1 nm QW, due to charge carrier transfer from the smaller QW through the thin c-AlN barrier into the wider QW.

Because of the indirect band gap of the 3C-SiC substrate no CL emission signal is detected at position 1. Spectrum 2 (blue curve) is assigned to the c-GaN buffer with an emission peak at 3.26 eV of the FX transition and a low emission signal at 3.64 eV. Spectrum 3 belongs to the c-AlN/GaN MQW structure nearest to the GaN buffer and shows two maxima at 3.26 eV and 3.60 eV with low intensity. Spectrum 4 represents the emission of the asymmetric c-MQWs at 3.64 eV near the surface in a defect reduced area. Here, the c-MQW emission intensity at 3.64 eV is drastically increased. The slightly higher

© 2015 WILEY-VCH Verlag GmbH & Co. KGaA, Weinheim

emission energy indicates that the thickness of the first QW may be about one monolayer wider than the QWs near the surface.

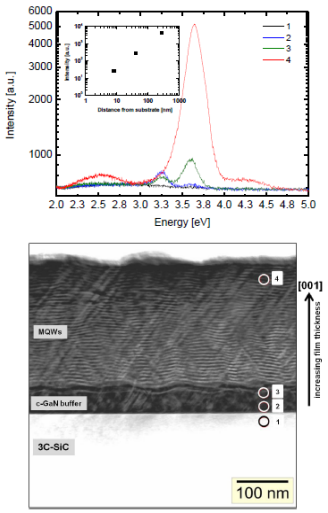

Figure 4 (a) Room temperature CL spectra recorded at the marked regions 1-4 in the STEM image in (b). In the inset the maximum intensities of the MQW peak at 3.64 eV from spectra 2-4 are plotted *versus* spot position from the 3C-SiC interface in a double logarithmic scale. (b) Cross-sectional ADF-STEM image taken along the [110] zone axis of sample B.

In the inset of Fig. 4a the maximum intensities of the MQW peak at 3.64 eV from spectra 2-4 are plotted *versus* the spatial position of the CL spot away from the 3C-SiC/c-GaN interface on a double logarithmic scale. A simple relationship between the spot position and the MQW emission intensity is clearly observed pointing out that the emission intensity increases with decreasing defect density. These results are in good qualitative agreement with the correlation of the FWHM of the rocking curves and the thickness in c-GaN layers plotted in Fig. 3. We observe a decreasing of the dislocation density N_{disl} and an increasing CL emission intensity with increasing film thickness.

4 Conclusion We have acquired and discussed correlated room temperature STEM/CL measurements from c-GaN and asymmetric c-GaN/AlN MQWs films. An increasing CL emission intensity with increasing film thickness due to the improved crystal quality was observed. This correlation can be connected to the reduction of the FWHM of X-ray ω-rocking curves with increasing film thickness of c-GaN films. SFs on the {111} planes are shown to lead to a decrease of the CL emission intensity.

Acknowledgements This work was supported by the DFG graduate program GRK 1464 “Micro- and Nanostructures in Optoelectronics and Photonics” as well as the Collaborative Research Center SFB 787 (project A8) and in the frame of the Research Instrumentation Program INST 272/148-1.

References

[1] P. Waltereit, O. Brandt, A. Trampert, H.T. Grahn, J. Menninger, M. Reiche, and K.H. Ploog, Nature **406,** 865 (2000).
[2] E. Tschumak, R. Granzer, J.K.N. Lindner, F. Schweiz, K. Lischka, H. Nagasawa, M. Abe, and D.J. As, Appl. Phys. Lett. **96**, 253501 (2010).
[3] C. Mietze, K. Lischka, and D.J. As, Phys. Status Solidi A **209**, 439 (2012).
[4] N. Zainal, S. V. Novikov, C. J. Mellor, C. T. Foxon, and A. J. Kent, Appl. Phys. Lett. **97**, 112102 (2010).
[5] S.V. Novikov, N.M. Stanton, R.P. Campion, C.T. Foxon, and A.J. Kent, J. Cryst. Growth **310**, 3964 (2008).
[6] A. Trampert, O. Brandt, H. Yang, and K. H. Ploog, Appl. Phys. Lett. **70**, 583 (1997).
[7] G. Feuillet, F. Widmann, B. Daudin, J. Schuler, M. Arlery, J.L. Rouviere, N. Pelekanos, and O. Briot, Mater. Sci. Eng. B **50**, 233 (1997).
[8] S. Sumnavadee, S. Sanorpim, B. Paosawat, and K. Onabe, J. Microsc. Soc. Thailand **24**, 136 (2010).
[9] Th. D. Moustakas, Phys. Status Solidi A **210**, 169 (2013).
[10] M. Albrecht, S. Christiansen, G. Salviati, C. Zanotti-Fregonara, Y. T. Rebane, Y. G. Shreter, M. Mayer, A. Pelzmann, M. Kamp, K. J. Ebeling, M. D. Bremser, R. F. Davis, and H. P. Strunk, MRS Symp. Proc. **468**, 293 (1997).
[11] R. Liu, A. Bell, and F.A. Ponce, Appl. Phys. Lett. **86**, 021908 (2005).
[12] G. Jacopin, L. Rigutti, L. Largeau, F. Fortuna, F. Furtmayr, F. H. Julien, M. Eickhoff, and M. Tschernycheva, J. Appl. Phys. **110**, 064313 (2011).
[13] J. Lähnemann, O. Brandt, U. Jahn, C. Pfüller, C. Roder, P. Dogan, F. Grosse, A. Belabbes, F. Bechstedt, A. Trampert, and L. Geelhaar, Phys. Rev. B **86**, 081302(R) (2012).
[14] F. Bertram, T. Riemann, J. Christen, A. Kaschner, A. Hoffmann, C. Thomsen, K. Hiramatsu, T. Shibata, and N. Sawaki, Appl. Phys. Lett. **74**, 359 (1999).
[15] T. Chassagne, A. Leycuras, C. Balloud, P. Arcade, H. Peyre, and S. Juillaguet, Mater. Sci. Forum **457-460,** 273 (2004).
[16] T. Schupp, K. Lischka, and D.J. As, J. Cryst. Growth **312**, 1500 (2010).
[17] J. Schörmann, S. Potthast, D.J. As, and K. Lischka, Appl. Phys. Lett. **90**, 041918 (2007).
[18] J. Christen, F. Bertram, G. Schmidt, S. Petzold, P. Veit, R. Ravash, A. Dadgar, and A. Krost, Micros. Microanal. **18**, (Suppl. 2), 1834 (2012)
[19] E. Martinez-Guerrero, E. Bellet-Almalric, L. Martinet, G. Feuillet, H. Mariette, P. Holliger, C. Dubois, C. Bru-Chevallier, P. Aboughe Nze, T. Chassagne, G. Ferro, Y. Monteil, and B. Daudin, J. Appl. Phys. **91**, 4983 (2002).
[20] J.E. Ayers, J. Appl. Phys. **78**, 3724 (1995).
[21] P. Gay, P.B. Hirsch, and A. Kelly, Acta Metall. **1**, 315 (1953).
[22] D. J. As, Proc. SPIE **7608**, 76080 G (2010).
[23] R.M. Kemper, C. Mietze, L. Hiller, T. Stauden, J. Pezoldt, D. Meertens, M. Luysberg, D.J. As, and J.K.N. Lindner, Phys. Status Solidi C **11**, 265 (2014).
[24] A. Belabbes, L.C. de Carvallo, A. Schleife, and F. Bechstedt, Phys. Rev. B **84**, 125108 (2011).
[25] C. Mietze, M.Bürger, S. Sakr, M. Tchernycheva, F. H. Julien, and D. J. As, Phys. Status Solidi A **210**, 455 (2013).
[26] S. Birner, C. Schindler, P. Greck, M. Sabathil, and P. Vogl, J. Comput. Electron. **8**, 267 (2009).

© 2015 WILEY-VCH Verlag GmbH & Co. KGaA, Weinheim